RSC Advances

ROYAL SOCIETY OF CHEMISTRY

www.rsc.org/advances

Cite this: DOI: 10.1039/c0xx00000x

www.rsc.org/xxxxxx

ARTICLE

The effects of Gallium on Solution-derived Indium Oxide-based Thin Film Transistors Manufactured on Display Glass

Chang-Ho Choi,[a] Yu-Wei Su,[a,c] Liang-Yu Lin,[d] Chun-Cheng Cheng[d] and Chih-hung Chang*[a]

Received (in XXX, XXX) Xth XXXXXXXXX 20XX, Accepted Xth XXXXXXXXX 20XX

DOI: 10.1039/b000000x

Metal oxide semiconductor TFTs have been considerably investigated as a promising alternative to hydrogenated amorphous silicon and organic semiconductors. While many multicomponent oxide TFTs have been studied, only a few reports of TFTs using amorphous indium gallium oxide channel layers. In this study, the effects of gallium atomic ratio on the performance of solution-derived indium oxide –based TFTs on display glass were investigated for the first time. The morphological, optical, and electrical properties of IGO channel layers with different gallium atomic ratios were characterized. IGO TFTs with various chemical compositions were compared and interpreted based on the analysis of In3d, Ga2p, and O1s XPS data. It was found that gallium dopant suppresses the generation of oxygen vacancy, while promoting the formation of oxygen in oxide lattice without oxygen vacancy by reducing the density of hydroxides. By adjusting the atomic ratio of gallium, we were able to fabricate the IGO TFTs on display glass with an average field-effect mobility as high as 6.1 cm^2/Vs, V_{on} = -2V, and on-off ratio of 10^7.

Introduction

Metal oxide semiconductors have been intensively researched over several decades due to their unique electrical and optical characteristics.[1, 2] Metal oxide semiconductors cover a wide range of optical band gaps including many materials with high optical transparency. In conjunction, metal oxide semiconductors with high-field effect mobility and excellent thermal/environmental durability appear to be a promising alternative to hydrogenated amorphous silicon and organic semiconductors for thin-film transistors (TFTs).[3, 4] In terms of manufacturing metal oxide semiconductors as an active channel layer for TFTs, vacuum deposition techniques such as sputtering, chemical vapor deposition, and atomic layer deposition have been generally employed—techniques which require higher capital cost and was constrained by lower throughput. Recently, metal oxide TFTs fabricated via solution-based processes have been pursued considerably for their potentials of offering simplicity, low cost, high throughput, and large area deposition.[5-12]

One of the most successful solution-based processes involves the dissolution of metal salt precursors in organic solvents, followed by coating or printing of the precursors onto device substrates to form the channel layers after converting the precursor films. Early examples were reported by Chang's group using metal halide precursors in acetonitrile solvent. Printed metal halide film absorbed H_2O in the air, which in turn formed metal hydroxyl halide film. During the thermal annealing step, the metal hydroxyl halide film was transformed to metal oxide through the removal of volatile by-product such as HCl. A variety of transparent semiconductor oxide thin films including ZnO, In_2O_3, SnO_2, ZnO–In_2O_3 (ZIO), In_2O_3–SnO_2 (ITO), ZnO–SnO_2 (ZTO), and In_2O_3–ZnO–SnO_2 (IZTO) have been fabricated using this process.[6, 7, 13] Taking advantages of simplicity and efficiency in preparing functional channel layers via solution-based processes, many researchers have reported a variety of metal oxide TFTs, ranging from binary to multicomponent channel layers. For example, Moon's group developed a solution formulation method in which metal organic salts were dissolved in 2-methoxyethanol (2-ME) and subjected to hydrolysis reaction during the precursor dissolution. They reported various metal oxide TFTs based on this approach, including SnOx, Zn-Sn-O (ZTO), and In-Ga-Zn-O (IGZO) TFTs.[14-17] Following these solution preparation approaches, many oxide TFTs studies have been reported in an effort to improving device performances and lowering the process temperature.[18-21] Binary oxide such as In_2O_3 and ZnO are popular choices of channel materials for TFTs. However it is challenging to control the electrical properties of these binary oxides for the fabrication of high performance TFTs. In_2O_3 tends to offer excess density of free electrons, resulting in In_2O_3 TFTs with higher values of field effect mobility along with higher leakage currents that require a negative gate voltage (V_g) to turn off the channel. On the other hand, TFTs with solution-processed ZnO channel layers, generally show lower values of field-effect mobility along with reasonable on-off ratios and V_{on} values. The use of multicomponent metal oxides provides an effective and convenient way to control the electrical properties of solution-processed channel layers by properly designing ratios of precursor component. Ga_2O_3, having strong bonding between gallium and oxygen, has a much lower density of free electrons than In_2O_3.[22] Thus, gallium has been used effectively in tailoring density of free electrons when In_2O_3 is used as a channel material. The addition of gallium could also result in dramatically lowering

processing temperatures for solution-derived indium zinc oxide thin-film transistors.[23]. Chiang *et al*. reported the fabrication of IGO TFTs via RF sputtering.[22] They varied the IGO film composition by changing the indium concentration to investigate the composition effects on the device performances. Fortunato *et al.* used RF sputtering to grow the IGO film at room temperature and investigated the variations of device performance on the effect of oxygen partial pressure.[24] Han *et al.* fabricated solution-derived IGO TFTs using inkjet printing technique to demonstrate the printed metal oxide TFTs.[13] Jeong *et al.* reported the impact of metal salt precursors in lowering process temperature of IGO TFTs.[25] Yu *et al.* fabricated In_2O_3/IGO bilayer TFTs, aimed at improving device performances and stability.[26] Using aqueous precursor solution, Hwang and Bae investigated the effect of gallium on indium oxide TFTs.[27] They varied the gallium concentration and discussed its effects on the device performances. To our best knowledge, there is no report on the effects of gallium on solution-derived indium oxide-based thin-film transistors manufactured on display glass. For practical applications of IGO films for TFTs manufacturing thus research results regarding IGO TFTs on display glass are valuable and meaningful. Although the deposition method is similar, dielectric and wetting properties of PECVD grown SiO_2 dielectric layer are different from those of thermally grown SiO_2, which eventually affects processing conditions and device performances. This difference is clearly shown in the contact angles data. The contact angles of acetonitrile on display glass with PECVD SiO_2 is around 9.36-13.35 and around 24.11-27.57 on thermally oxidized silicon coupons.

In this study, we fabricated TFTs on display glass substrate using amorphous IGO channel layers, varying the amount of gallium component to investigate the gallium effect on the device performances. The IGO films were formed by depositing metal salt precursor solution onto the substrate and annealed at 500 °C for 2 hours in atmospheric conditions. By exploring the concentration of gallium, we obtained the device performances with an average field-effect mobility value as high as 6.1 cm^2/Vs, V_{on} = -2V, and on-off ratio of 10^7.

Experimental

Device fabrication

A molybdenum (Mo) layer with 200 nm thickness was formed onto display glass substrate for a gate electrode by using sputtering deposition, and then deposition of SiO_2 dielectric layer with a thickness of 100 nm was carried out by PECVD process. The breakdown voltage of the PECVD SiO_2 dielectric layer was measured to be greater than 15 MV/cm at 1 MV/cm. The leakage current of the dielectric layer at 1MV/cm was also measured to be 4.5 nA/cm^2. The capacitance of the dielectric layer was measured to be 191 nF/cm^2 at 1 kHz, resulting in a permittivity of 5.1. The substrates were treated using O_2 plasma cleaning prior to the deposition. $In(NO_3)_3$ anhydrous salt and $Ga(NO_3)_3$ hydrate were purchased from Alfa Aesar. A solvent of 2-methoxyethanol (2-ME) was purchased from Fisher Scientific. All chemicals were used without further purification process. $In(NO_3)_3$ and $Ga(NO_3)_3$ precursors were dissolved in 2-ME solvent, and ratios of two precursor were varied by changing the gallium precursor concentration. While 0.05 M $In(NO_3)_3$ was set, $Ga(NO_3)_3$ concentration of 0.005 M, 0.01 M, 0.025 M, and 0.05 M was added to make a precursor ratio of 10:1, 5:1, 2:1, and 1:1 respectively. The precursor solution was spin-coated at 4500 RPM for 30 seconds. As-deposited film was dried on a hot plate at 120 °C for 30 minutes, allowing solvent to evaporate. The film was then annealed at 500 °C in the air for 2 hours. IGO films were patterned by using a photolithography process. The patterned samples were dried on a hot plate at 120 °C prior to the deposition of Al source and drain. The source and drain were deposited by thermal evaporation using a shadow mask for patterning. The active channel layer was defined at 1200 μm and 200 μm for width and length, respectively.

Characterization

Device characterization was performed in ambient condition using Agilent Technologies E5270B Semiconductor Parameter Analyzer. Electrical performances of devices were assessed by testing at least 30 devices prepared in each gallium concentration. The morphology and roughness of the films were analysed using atomic force microscope (AFM, Veeco Nanoscope digital instruments). The optical properties of the films were studied using UV-vis spectroscopy (Jasco, V-670 Spectrophotometer). For the transmittance measurement, IGO film was deposited on bare soda lime glass substrate. X-ray diffraction (XRD, Bruker D8 discover) was used to study the crystallinity of the films. X-ray photoelectron spectroscopy (XPS, ESCALAB 200-IXL instrument with Mg K radiation) was employed to investigate elemental composition of the films. High-resolution transmission electron microscopy (HRTEM, FEI TITAN 80-200) equipped with fast Fourier transform (FFT) was used to measure the thickness and crystallinity of the film. For the preparation of HRTEM specimen of the IGO film, a focus ion beam (FIB) process was employed. Chromium, platinum, and carbon layer were intentionally coated on the IGO film during the FIB process to protect and contrast the film.

Results and Discussion

Figure 1 displays the HRTEM image of IGO (In:Ga = 10:1) film along with the FFT pattern. The thickness of the film was measured to be around 10 nm. The TEM image indicates that the film was uniform, dense, and continuous without forming any pores. The film appears to be amorphous according to the FFT pattern (Figure 1b). It is generally known that with an elevated annealing temperature, film tends to increase its crystallinity. However, the IGO films appear to be amorphous even after annealing at 500 ^oC for 2 hours. It is believed that this result is likely related to the thin thickness of the IGO films. Because the IGO film is in direct contact with the SiO_2 dielectric layer, the crystallinity of the IGO film is expected to be affected by the amorphous structure of the dielectric layer. It has been reported that the crystallinity of film having a direct contact with the surface of dielectric layer is dictated by the phase of the dielectric layer, while the crystallinity of film further away from the dielectric layer surface is affected more by the processing conditions other than the dielectric layer surface structure.[28, 29]

The film formed on the surface of the dielectric layer favors to relax by matching its structure to that of the dielectric layer and as a result avoid the formation of interfacial defects. The IGO films in this study are very thin (~10 nm thickness) and appear to be amorphous, indicating that the crystallinity of the film was likely influenced by the amorphous SiO_2 dielectric layer.

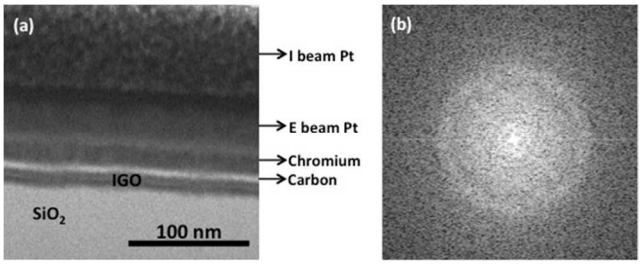

Fig.1. HRTEM image of 10:1 IGO film.

The XRD patterns also confirm the IGO films are amorphous, regardless of the amount of gallium mole fraction. A represented XRD diffractogram of the IGO films is shown in Figure 2. No visible peak of the crystalline IGO phases could be observed except a broad peak from the glass substrate.

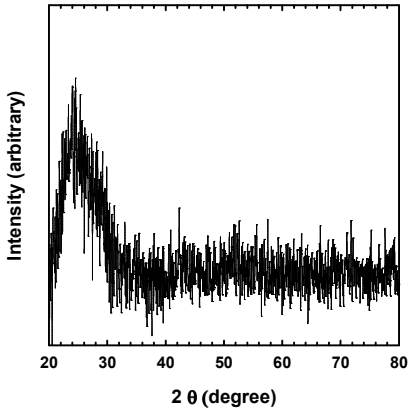

Fig.2. XRD diffractogram of 10:1 IGO film.

Figure 3 displays the AFM images of the IGO films fabricated with different amounts of gallium. The films are smooth and uniform with values of average roughness from 0.4 to 1.7 nm. No grains or particulates are clearly visible from these images, confirming the amorphous structure of these films. The AFM analysis indicates that the gallium mole fraction does not have a significant impact on the morphology of IGO films.

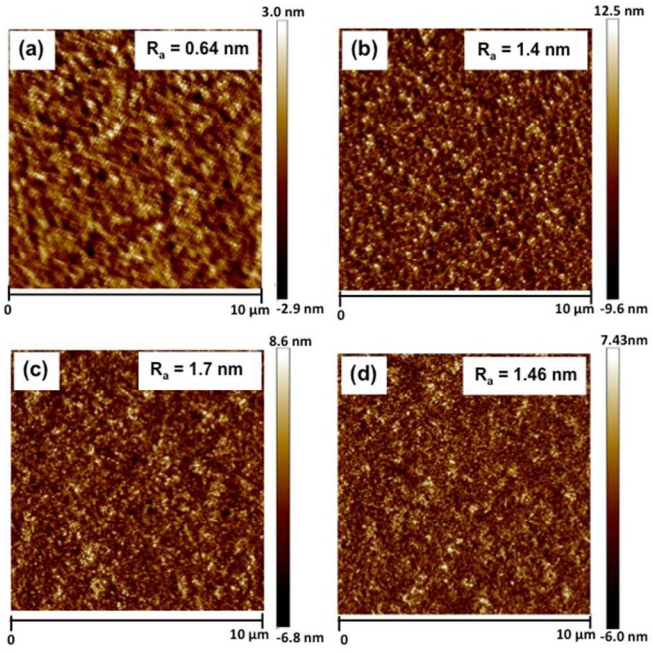

Fig.3. AFM images of IGO film with various In:Ga ratios of (a) 10:1, (b) 5:1, (c) 2:1, and (d) 1:1.

The optical properties of IGO films with different Ga mole fraction were characterized by UV-Vis spectrophotometer and the results are shown in Figure 4. The estimated optical band gap of the film is dependent upon the gallium mole fraction, exhibiting a value range from 3.6 to 3.8 eV. With the gallium mole fraction from 10 to 20%, the band gap was measured to be around 3.6 eV. As the gallium mole fraction was increased over 20 %, the band gap gradually increased and reached up to around 3.8 eV. Minami *et al.* reported the preparation of Ga_2O_3-In_2O_3 films with various gallium amounts by using dc and rf sputtering.[30, 31] They studied the correlation of crystallographic, electrical, and optical properties of the resultant films with gallium mole fraction. They observed the transition of the crystal structure of the film from Ga-incorporated In_2O_3 solid solution to a ternary compound of $(Ga_{1-x},In_x)_2O_3$. As the transition occurred, the band gap began to increase with the increase of gallium amount. Particularly the band gap increased sharply, as the gallium reached over 50 %. Although crystallographic study is not available for our amorphous IGO films, it may be reasonable to assume the same phase transition to occur in our IGO films with high gallium contents, based on the analysis of the band gap. High transmittance in visible range was observed from 10:1 IGO film as shown in Figure 4 b, assuring the use of the IGO films for transparent semiconducting electronics.

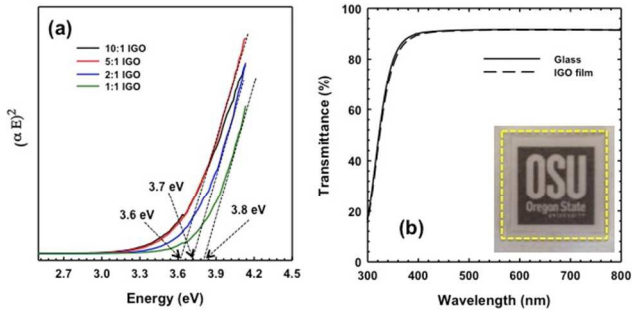

Fig.4. Optical properties of IGO films: (a) band gap measurement of IGO films with various gallium amounts and (b) transmittance in visible range of 10:1 IGO film (inset: optical image of transpatrent IGO film).

The represented electrical performances of the IGO TFTs fabricated using different gallium mole fraction are given in Figure 5 for comparison. We first fabricated binary In_2O_3 TFTs at 500 °C and measured their electrical characteristics.[32] It was found that the binary In_2O_3 TFTs were not able to turn off with a reasonable gate voltage (V_g) value.

Adding the gallium amount by 10 % into In_2O_3 (10:1) led to the fabrication of operational transistors. However, the channels were still conductive, with on-off ratios of 10^3~$10^{4.5}$, V_{on} of -24~-10V, and operated as depletion mode transistors (Figure 5 a and b). Relative to the On current value, the Off current value is high, leading to low on-off ratios. There are several models to extract the mobility of TFTs. While each model has its characteristics in extracting the mobility, we adopted a field effect mobility model that is commonly used and obtained by transconductance at low V_{ds}. The model to extract the field effect mobility is following.

$$\mu_{FE} = \frac{g_m}{C_i \frac{W}{L} V_{ds}}$$

Where g_m is transconductance, C_i is capacitance of gate insulator layer, W and L is width and length of channel respectively, and V_{ds} is the applied drain voltage. In this study, drain voltage of V_{ds} =1V was applied for the field effect mobility extraction. The mobility of the devices with 10:1 ratio was 4.5 ± 2.2 cm^2/Vs.

We increased the gallium atomic ratio to 20 % to fabricate 5:1 IGO channel layer and assessed the electrical performances. The results are given in Figure 5 c and d. Compared with the electrical performances of TFTs using 10:1 IGO channel layers, the devices could be switched off at relatively low gate voltages (V_{on}=-16~-2V) and correspondingly showed high values of on-off ratio from $10^{5.5}$ to 10^7. The improved on-off ratio is attributed to the significant decrease of the Off-current (2.0×10^{-7} → 1.6×10^{-9} A). The output characteristic curve also indicates that the 5:1 IGO channel is less conductive than that of the 10:1 IGO channel, exhibiting a clear current saturation at high drain voltage (V_{ds}). The average mobility was calculated to be around 6.1 ± 0.9 cm^2/Vs.

Adding more gallium to prepare TFTs with a channel layer of 2:1 IGO, the channels became less conductive, turning the depletion mode transistor to the enhancement mode one (Figure 5 e and f). The devices now turned on with a positive turn-on voltage (V_{on}) of 0~2V. The Off-current value dropped to 1.6×10^{-11} and the on-off ratio was further improved to $10^{6.5}$ ~ $10^{7.5}$. The average mobility was estimated to be around 3.7 ± 0.6 cm^2/Vs.

Lastly we fabricated IGO films using solutions with equal molar concentration of In and Ga salt (Figure 5 g and h). The devices showed a lower average mobility value around 0.7 ± 0.4 cm^2/Vs, on-off ratio of $10^{4.5}$ ~ $10^{5.5}$, and V_{on}= 2~10 V. The on-current value at high drain voltage (V_{ds}) was reduced as shown in output characteristic curve (Figure 5 h).

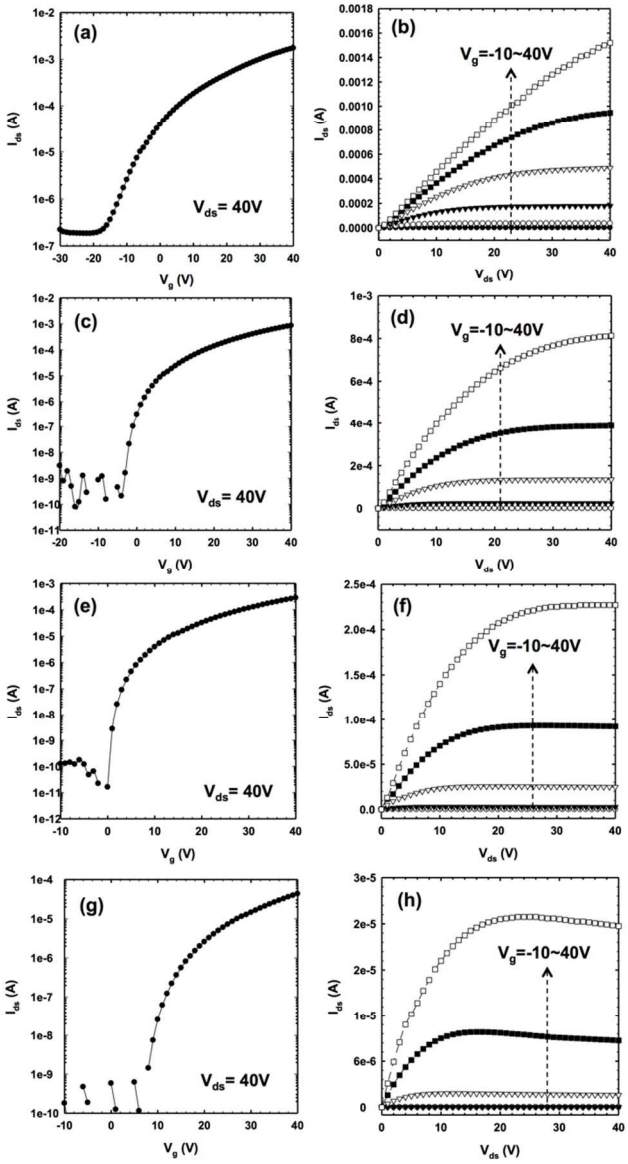

Fig.5. Transfer and output characteristic curves of IGO TFTs with various In:Ga ratios of 10:1 (a, b), 5:1 (c, d), 2:1 (e, f), and 1:1 (g, h).

The device performances of the IGO films fabricated with different chemical compositions are summarized in Table 1. After analyzing the obtained device performances, we were able to summarize the effects of gallium mole fraction on the device performances. As more gallium was added, the conductivity of the channel decreased, transforming the transistors from the depletion mode to the enhancement mode, along with an improved on-off current ratio. As the mole fraction of gallium reach 50%, the TFTs operated relatively poor, suggesting the optimal gallium mole fraction to yield high performance IGO

TFTs is between 20% to 30%. The V_{on} value has a relatively wide range in each device condition. Generally V_{on} value is dependent upon the electron density. With the fact that the Ga element determines the degree of oxygen vacancies and thus electron density, a uniform Ga element content over the film should lead to a narrow range of V_{on} value. However, the Von value also depends on the channel layer thickness. During spin-coating of the metal salt solution onto the substrate, the film thickness may not be uniform over the substrate, which would result in variations over the channel thickness and correspondingly wide range of V_{on} values.

Table 1. Device performance summary of IGO TFTs with different In:Ga ratios.

Devices (In:Ga)	Mobility (cm^2/Vs)	Von (V)	On/Off ratio
10:1	4.5 ± 2.2	-24 ~ -10	10^3~$10^{4.5}$
5:1	6.1 ± 0.9	-16 ~ -2	$10^{5.5}$~10^7
2:1	3.7 ± 0.6	0 ~ 2	$10^{6.5}$ ~ $10^{7.5}$
1:1	0.7 ± 0.4	2 ~ 10	$10^{4.5}$ ~ $10^{5.5}$

In order to elucidate the gallium effects on the indium-oxide based TFTs performances, we analysed the chemical composition and electronic structure of the IGO films using XPS. Figure 6 shows the XPS of In3d and Ga2p of IGO films prepared at various gallium concentrations. The In3d core level peaks at 445 eV and 452 eV appeared, which is attributed to spin-orbit split $3d_{5/2}$ and $3d_{3/2}$.[33] The peaks correspond to the In^{3+} oxidation state, indicating the formation of In_2O_3. Ga 2p core level spectrum was shown at 1118.1 eV and 1118.9 eV for the low gallium concentrations (10:1 and 5:1) and high gallium concentrations (2:1 and 1:1) respectively. The peak at 1118.1 eV perfectly fits to Ga^{3+} oxidation state. The peak shifts to higher binding energy at high gallium concentrations indicates that gallium affects the core level binding energy of gallium. However, the shift does not present the different oxidation state of gallium such as Ga^0 and Ga^{1+} because the binding energy of these low oxidation states of gallium oxide is generally shown at 1116.7 eV and 1117.7 eV respectively.[34] The chemical compositions of the IGO film are summarized in Table 2. The composition ratios of indium to gallium were found to be 13.7, 7.0, 5.4, and 1.8 as the gallium amount increases from 10 to 50 %. The composition ratio of the film is inversely proportional to the added gallium amounts in the solution preparation although the stoichiometry of the resultant films is deviated from the concentrations of indium and gallium precursor solution. Such a deviation may be attributed to film preparation. Prior to dispersing the metal salt solution onto the substrate, we filtered the solution with a syringe filter to remove any undissolved precursors. In this process, we might lose some portion of precursors. Since the $Ga(NO_3)_3$ precursor is hydrated, it is possible for the formation of $Ga(OH)_3$ particles that got filtered out.

The O1s XPS spectra of the IGO film with different gallium atomic ratios are shown in Figure 7. The O1s XPS was de-convoluted into three peaks. The peaks at near 531 eV and 532 eV are assigned to the oxygen in the oxide lattice without oxygen vacancy and with oxygen vacancy respectively.[18, 23, 26] The peak with higher binding energy at 533 eV arise from hydroxide atoms.[18] The O1s XPS data of the IGO films with various compositions are compared in Table 2. As clearly displayed in Figure 7, the 10:1 IGO film contains relatively large amount of oxygen vacancies and hydroxides. As more gallium atoms were added, the concentration of coordinated oxygen increased while the concentration of oxygen vacancy was suppressed. The suppression of oxygen vacancy is attributed to strong bonding of gallium to oxygen. The creation of hydroxides also appears to be affected by the addition of gallium. Jeong *et al.* reported the effect of adding gallium in lowering the annealing temperatures for the fabrication of solution-derived metal oxide TFTs.[23] They claimed that the addition of gallium promoted the filling of oxygen in oxide lattice at an annealing temperature as-low-as 250 °C, while retaining the creation of hydroxides. Since the generation and transportation of charge carriers occur in a chemical composition of heavy metal cation (ns-orbital) and oxygen (2p-orbital), not definitely hydroxide, the transition from hydroxide to oxide is critical in terms of manufacturing high performance transistors.[35, 36] We believe that a similar effect of gallium addition is being observed in our IGO TFTs even though they were annealed at a higher temperature.

Table 2. Summary of chemical compositions of IGO films

10:1 IGO TFTs					
Element	In3d	Ga2p	O_o	V_o	M-OH
Atom (%)	6.7	0.5	30.8	16.2	8.6
5:1 IGO TFTs					
Element	In3d	Ga2p	O_o	V_o	M-OH
Atom (%)	10.3	1.5	45.3	7.0	2.9
2:1 IGO TFTs					
Element	In3d	Ga2p	O_o	V_o	M-OH
Atom (%)	10.8	2.0	47.5	5.3	2.7
1:1 IGO TFTs					
Element	In3d	Ga2p	O_o	V_o	M-OH
Atom (%)	12	6.3	48.3	4.8	2.1

For the TFTs with a 10:1 In:Ga atomic ratio, the density of charge carriers (free electrons) is high due to the large amount of oxygen vacancies, which resulted in forming depletion mode transistors as shown in Figure 5 a. In general, high density of oxygen vacancies is preferred to improve the field effect mobility since charge carrier, generated by oxygen vacancy, transports by percolation conduction after filling trap states. Despite the high density of oxygen vacancies, the 10:1 IGO TFTs did not yield the greatest mobility.

There may be two major factors leading to these results. As mentioned earlier in the XPS data analysis, the high density of hydroxides deteriorates the device performances. Another factor may be associated with ionized impurity scattering. Several quantitative models have been proposed to explain the electronic transport properties of metal oxide films, including ionized impurity scattering, grain boundary scattering, and lattice vibration scattering.[37] Since the IGO channel layers were amorphous, the electron transportation is insensitive to the grain boundary scattering. According to the transfer curves and XPS O1s spectra, the 10:1 IGO film contains high density of oxygen vacancies. The high density of oxygen vacancies which could behave as ionized scattering centers and resulted in lowering

field-effect mobility.[37, 38]

Based on the results of device performances and XPS data, it was suggested that IGO TFTs with a 5:1 In:Ga atomic ratio yield the best device performances with the greatest mobility and decent V_{on} and on-off ratio. The improved device performances result from the significant increase of metal coordinated oxygen without oxygen vacancy, along with a significant decrease of hydroxides compared with those of the 10:1 IGO TFTs. As more gallium is added, the chemical composition of the IGO films altered with a constant trend. More gallium adding increases oxygen contents without oxygen vacancy, while decrease the density of oxygen vacancies and hydroxides. These results correspond to the shift of V_{on} from a negative to a positive value and a decrease of mobility value from for 2:1 and 1:1 IGO TFTs. For the 1:1 IGO TFTs, the device performances, especially mobility, considerably deteriorate due to the insufficient density of oxygen vacancies. Additionally, the decrease of On-current at high gate bias (V_g= 30 ~ 40) was observed at a high drain voltage (V_{ds}). This phenomenon, referred to as a negative differential resistance (NDR), has been discussed in various types of transistors.[32, 39, 40] Although the NDR phenomena could originate from a variety of routes, researchers suggested that it is likely to be caused by the density of trap states that would originate from self-heating, carrier trapping, and impurities. The IGO TFTs with a 1:1 In:Ga atomic ratio, the channel layer does not possess sufficient charge carriers available for the current generation after filling the trap states at high gate and drain applied bias. The formation of ternary compound of $(Ga_{1-x}In_x)_2O_3$ could act as impurities, which may be a potential cause of NDR.

Jeong *et al.*. performed a careful study using the same precursor formulation method of this current study by varying the gallium content. The IGO TFTs were fabricated on thermally grown SiO_2 layer on Si at an annealing temperature of 300 °C.[25] Their champion device shows a mobility of 1 cm2/Vs obtained with a gallium content of 6 %, and the mobility decreased with an increase of the gallium content. These results are quite different from the current findings. The use of different substrate is likely the key cause of the difference.

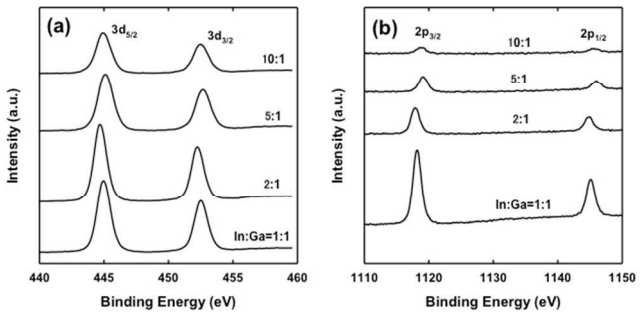

Fig.6. XPS In3d and Ga2p spectra of IGO film with various chemical compositions.

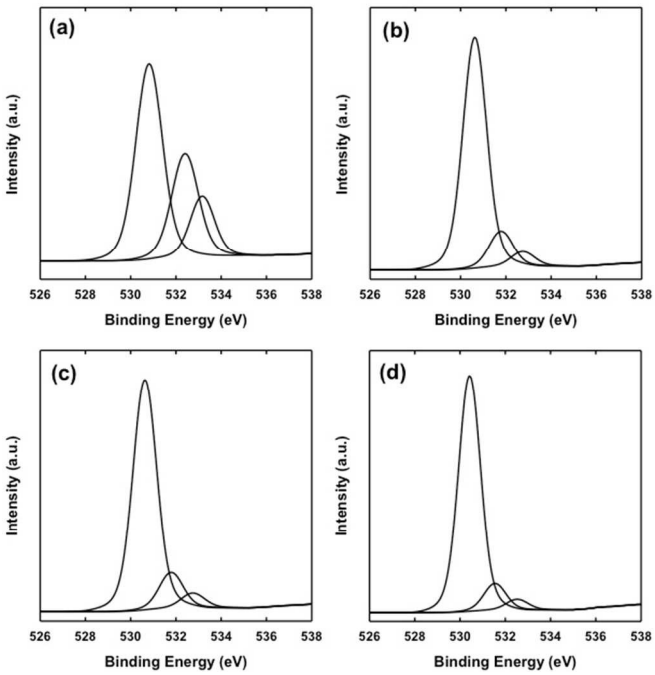

Fig.7. XPS O1s spectra of IGO film with various chemical compositions.

Conclusions

TFTs with amorphous indium gallium oxide channel layers were fabricated on display glass substrate via a metal salt route. The IGO TFTs with different In:Ga atomic ratios were prepared by simply changing the gallium precursor amount while fixing the indium precursor amount. The morphological, optical, and electrical properties of IGO TFTs were characterized, along with the study of chemical composition based on the XPS data. It was found that gallium atomic ratio significantly altered the electrical performances of the IGO TFTs. The addition of gallium turned the non-switchable In_2O_3 TFTs into operational transistors, suppressing the generation of oxygen vacancies. The addition of gallium also promoted the formation of oxygen in oxide lattice without oxygen vacancies while reducing hydroxides. These combined effects resulted in IGO TFTs using channel layers with a In:Ga ratio of 5:1 to show the best device performances among others that were tested in this study.

Acknowledgement

This research is funded by AU Optronics Corporation. Zhen's help in depositing aluminium electrode contacts is highly appreciated. The TEM is funded by National Science Foundation via the Major Research Instrumentation (MRI) Program under Grand No. 1040588.

Notes and references

[a] *Address, Address, Town, Country. Fax: XX XXXX XXXX; Tel: XX XXXX XXXX; E-mail: xxxx@aaa.bbb.ccc*
[b] *Address, Address, Town, Country. Fax: XX XXXX XXXX; Tel: XX XXXX XXXX; E-mail: xxxx@aaa.bbb.ccc*

† Electronic Supplementary Information (ESI) available: [details of any supplementary information available should be included here]. See DOI: 10.1039/b000000x/

‡ Footnotes should appear here. These might include comments relevant to but not central to the matter under discussion, limited experimental and spectral data, and crystallographic data.

1 A. Name, B. Name and C. Name, *Journal Title*, 2000, **35**, 3523; A. Name, B. Name and C. Name, *Journal Title*, 2000, **35**, 3523.

1. E. Fortunato, P. Barquinha and R. Martins, *Adv. Mater.*, 2012, **24**, 2945-2986.
2. J.-Y. Kwon, D.-J. Lee and K.-B. Kim, *Electron. Mater. Lett.*, 2011, **7**, 1-11.
3. K. Nomura, H. Ohta, A. Takagi, T. Kamiya, M. Hirano and H. Hosono, *Nature*, 2004, **432**, 488-492.
4. E. M. C. Fortunato, P. M. C. Barquinha, A. Pimentel, A. M. F. Goncalves, A. J. S. Marques, L. M. N. Pereira and R. F. P. Martins, *Advanced Materials*, 2005, **17**, 590-594.
5. S. Jeong and J. Moon, *J. Mater. Chem.*, 2012, **22**, 1243-1250.
6. D.-H. Lee, S.-Y. Han, G. S. Herman and C.-H. Chang, *J. Mater. Chem.*, 2009, **19**, 3135-3137.
7. D.-H. Lee, Y.-J. Chang, G. S. Herman and C.-H. Chang, *Adv. Mater.*, 2007, **19**, 843-847.
8. G. Adamopoulos, A. Bashir, S. Thomas, W. P. Gillin, S. Georgakopoulos, M. Shkunov, M. A. Baklar, N. Stingelin, R. C. Maher, L. F. Cohen, D. D. C. Bradley and T. D. Anthopoulos, *Adv. Mater.*, 2010, **22**, 4764-4769.
9. C. Avis and J. Jang, *J. Mater. Chem.*, 2011, **21**, 10649-10652.
10. H. S. Kim, P. D. Byrne, A. Facchetti and T. J. Marks, *J. Am. Chem. Soc.*, 2008, **130**, 12580-12581.
11. M.-G. Kim, H. S. Kim, Y.-G. Ha, J. He, M. G. Kanatzidis, A. Facchetti and T. J. Marks, *J. Am. Chem. Soc.*, 2010, **132**, 10352-10364.
12. C.-H. Choi, L.-Y. Lin, C.-C. Cheng and C.-h. Chang, *ECS J. Solid State Sc.*, 2015, **4**, P3044-P3051.
13. S.-Y. Han, D.-H. Lee, G. S. Herman and C.-H. Chang, *J.Disp. Technol.*, 2009, **5**, 520-524.
14. S. Jeong, Y. Jeong and J. Moon, *J. Phys. Chem. C*, 2008, **112**, 11082-11085.
15. K. Song, D. Kim, X.-S. Li, T. Jun, Y. Jeong and J. Moon, *J. Mater. Chem.*, 2009, **19**, 8881-8886.
16. D. Kim, C. Y. Koo, K. Song, Y. Jeong and J. Moon, *Appl. Phys. Lett.*, 2009, **95**. 103501.
17. Y. Jeong, K. Song, D. Kim, C. Y. Koo and J. Moon, *J. Electrochem. Soc.*, 2009, **156**, H808-H812.
18. S.-Y. Han, G. S. Herman and C.-h. Chang, *J. Am. Chem. Soc.*, 2011, **133**, 5166-5169.
19. M.-G. Kim, M. G. Kanatzidis, A. Facchetti and T. J. Marks, *Nature Materials*, 2011, **10**, 382-388.
20. K. K. Banger, Y. Yamashita, K. Mori, R. L. Peterson, T. Leedham, J. Rickard and H. Sirringhaus, *Nat. Mater.*, 2011, **10**, 45-50.
21. Y.-H. Kim, J.-S. Heo, T.-H. Kim, S. Park, M.-H. Yoon, J. Kim, M. S. Oh, G.-R. Yi, Y.-Y. Noh and S. K. Park, *Nature*, 2012, **489**, 128-132.
22. H. Q. Chiang, D. Hong, C. M. Hung, R. E. Presley, J. F. Wager, C. H. Park, D. A. Keszler and G. S. Herman, *J. Vac. Sci. Technol. B*, 2006, **24**, 2702-2705.
23. S. Jeong, Y.-G. Ha, J. Moon, A. Facchetti and T. J. Marks, *Adv. Mater.*, 2010, **22**, 1346-1350.
24. G. Goncalves, P. Barquinha, L. Pereira, N. Franco, E. Alves, R. Martins and E. Fortunato, *Electrochem. Solid-State Lett.*, 2010, **13**, H20-H22.
25. S. Jeong, J.-Y. Lee, S. S. Lee, Y. Choi and B.-H. Ryu, *J. Phys. Chem. C*, 2011, **115**, 11773-11780.
26. X. Yu, N. Zhou, J. Smith, H. Lin, K. Stallings, J. Yu, T. J. Marks and A. Facchetti, *ACS Appl. Mater..Inter.*, 2013, **5**, 7983-7988.
27. Y. H. Hwang and B.-S. Bae, *J.Disp. Technol.*, 2013, **9**, 704-709.
28. H.-H. Hsieh and C.-C. Wu, *Appl. Phys. Lett.*, 2007, **91**, **013502**.
29. K. S. Ahn, Y. C. Nah and Y. E. Sung, *J. Vac. Sci. Technol. A*, 2002, **20**, 1468-1474.
30. T. Minami, S. Takata and T. Kakumu, *J.Vac. Sci..Technol. A*, 1996, **14**, 1689-1693.
31. T. Minami, Y. Takeda, T. Kakumu, S. Takata and I. Fukuda, *J. Vac. Sci. Technol. A*, 1997, **15**, 958-962.
32. C.-H. Choi, S.-Y. Han, Y.-W. Su, Z. Fang, L.-Y. Lin, C.-C. Cheng and C.-h. Chang, *J. Mater. Chem. C*, 2015, **3**, 854-860.
33. J. Gan, X. Lu, J. Wu, S. Xie, T. Zhai, M. Yu, Z. Zhang, Y. Mao, S. C. I. Wang, Y. Shen and Y. Tong, *Sci. Rep.*, 2013, **3**, 1021.
34. W. Priyantha, G. Radhakrishnan, R. Droopad and M. Passlack, *J.Cryst. Growth*, 2011, **323**, 103-106.
35. H. Hosono, *J.Non-Cryst. Solids*, 2006, **352**, 851-858.
36. H. Hosono, N. Kikuchi, N. Ueda and H. Kawazoe, *J.Non-Cryst. Solids*, 1996, **200**, 165-169.
37. H. Nakazawa, Y. Ito, E. Matsumoto, K. Adachi, N. Aoki and Y. Ochiai, *J.Appl. Phys.*, 2006, **100**, 093706.
38. J. R. Bellingham, W. A. Phillips and C. J. Adkins, *J Phys. Condens. Matter*, 1990, **2**, 6207-6221.
39. S. Dasgupta, R. Kruk, N. Mechau and H. Hahn, *ACS Nano*, 2011, **5**, 9628-9638.
40. J. Lee, M. J. Panzer, Y. He, T. P. Lodge and C. D. Frisbie, *J. Am. Chem. Soc.*, 2007, **129**, 4532-4533.